ACS APPLIED NANO MATERIALS

www.acsanm.org Article

Layered Assembly of Silver Nanocubes/Polyelectrolyte/Gold Film as an Efficient Substrate for Surface-Enhanced Raman Scattering

Qiang Wang, Xiuhui Bai, Yang Zhang,* Ziang Zhou, Ming Guo, Jiatao Zhang,* Chunhong Li, Changzheng Wang,* and Shaowei Chen

Cite This: *ACS Appl. Nano Mater.* 2020, 3, 1934−1941 Read Online

ACCESS | Metrics & More | Article Recommendations | Supporting Information

ABSTRACT: Surface-enhanced Raman scattering (SERS) is of great importance for the sensitive, rapid, and repeatable detection of target analytes. The electromagnetic enhancement has a major contribution to the signal enhancement in SERS which is critically dependent on the micro-/nanomorphology of noble metal (e.g., Au and Ag) film substrates. Herein, Ag nanocubes/polyelectrolyte/Au (Ag/PE/Au) sandwich-structured film is fabricated by the layer-by-layer deposition and then utilized as an efficient SERS substrate by the coupling of localized surface plasmons (LSPs) and surface plasmon polaritons (SPPs) resonances while the electromagnetic field enhancement is confined within the PE gap layer which is sandwiched between Ag nanocubes and Au film. With rhodamine 6G and crystal violet as the probe molecules, the Ag/PE/Au sandwich-structured film demonstrates highly sensitive SERS signals, which is further supported by the theoretical simulations as well. This work indicates that the Ag/PE/Au sandwich-structured film can be employed as a reliable SERS substrate for sensitive molecular sensing applications.

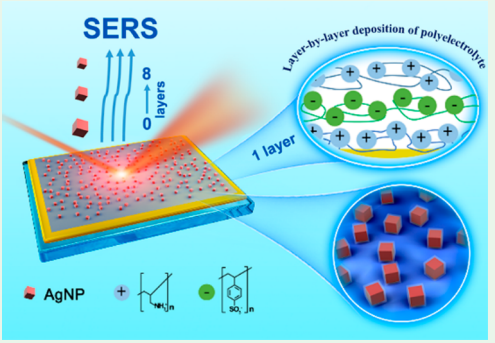

KEYWORDS: *surface-enhanced Raman scattering (SERS), Ag nanocubes, sandwiched nanostructures, LSP resonances, SPP resonances*

1. INTRODUCTION

Surface-enhanced Raman scattering (SERS) has been attracting extensive interests, as it is a unique technique that can afford a rapid, sensitive, nondestructive, label-free detection of a wide range of molecular analytes.[1−3] SERS effect was first reported by Fleischmann et al. in 1973 with pyridine adsorbed on electrochemically roughened silver surface.[4] The Raman amplification depends on chemical and electromagnetic enhancement that in general arises from roughened metal surfaces (e.g., Cu, Ag, Au, etc.).[5−7] The electromagnetic fields close to the rough metal surface can be drastically enhanced through the excitation of localized surface plasmons (LSPs), which is a critical factor for SERS applications.[8−10] In the past decade, various SERS substrates have been explored to boost the sensitivity of SERS toward meeting the demand for efficient detection of single molecule.[11−14] According to previous reports, the achievement of strongest SERS performance relies on the regions of the electromagnetic field that are highly concentrated by plasmonic metallic nanoparticles or the gaps between nanostructures and analyte molecules. Tremendous efforts have been devoted to fabrication techniques which can accurately control the distance within a few nanometers for investigating the interparticle coupling effect on SERS.[15,16]

In particular, a more pronounced enhancement can be achieved by either the fabrication of plasmonic nanostructures or assembly of plasmonic nanomaterials.[17,18] In general, nanomaterials with sharp edges demonstrate higher SERS activity than those of spherical nanoparticles associated with the presence of greater electric fields. For instance, Ag nanocubes with good monodispersity were used for the fabrication of SERS substrates due to an enhancement of the electromagnetic field.[19] The LSP absorption can be regulated by several structural parameters, including the shape, size, and crystal structure of metal nanoparticles, interparticle distance, and dielectric properties of the metal and the surface media, respectively.[20−24] However, significant challenges still remain due to the complicated self-assembly process, unfavorable aggregation, and low reproducibility.[25]

Recent reports have pointed out that the electromagnetic field could be further utilized, and that metallic nanoparticles could be positioned over a metal film, through precisely tuning the gap between the film and nanoparticles.[26,27] In principle, the LSPs and SPPs can coexist at the boundaries between dielectric and conductive materials, resulting from the metallic nanoparticles and periodical metal nanostructures. Previous work revealed that the electromagnetic field can be confined and enhanced in the gap due to the hybridization of SPP and LSP resonance as the metallic nanoparticles were placed near a

Received: December 23, 2019
Accepted: January 21, 2020
Published: January 21, 2020

https://dx.doi.org/10.1021/acsanm.9b02579
ACS Appl. Nano Mater. 2020, 3, 1934−1941

metal film with a nanoscale gap.[28,29] Therefore, the electromagnetic coupling can be further employed to improve the detection sensitivity via SERS, holding a promising potential for the design and fabrication of a large-scale device.[30]

In this work, we demonstrate a convenient and efficient method to fabricate a Ag nanocubes/polyelectrolyte/Au film (Ag/PE/Au) sandwiched structure by randomly dispersing as-synthesized Ag nanocubes on the nanometer thickness polymer spacer layer. Ag nanocubes were assembled on the PE layer surface without using any additional process to control their spatial arrangement.[31−34] An accurate distance between as-deposited Ag nanocubes and underlying Au films was fabricated by a layer-by-layer deposition of PE layers. Remarkable enhancement in SERS signals was experimentally achieved through the rationally designed SERS substrate and probe molecules (rhodamine 6G and crystal violet) due to the coupling of multiple LSP and SPP resonances.[35−39] A high degree of morphological, size, and distance control facilitates a better understanding of the enhancement mechanisms in SERS and search for optimal conditions. The electromagnetic enhancement was further investigated by the finite-difference time-domain simulations.

2. EXPERIMENTAL SECTION

2.1. Chemicals. Ethylene glycol (A.R.), poly(vinylpyrrolidone) (PVP, $M_r \approx 58000$), poly(allylamine) hydrochloride (PAH, M_w = 70 kDa, Aldrich), HCl (36.0−38.0 wt %), $AgNO_3$ (≥99.8%, A.R.), carbamide ($CO(NH_2)_2$, ≥99%, A.R.), polystyrenesulfonate (PSS, M_w = 70 kDa, Aldrich), rhodamine 6G (R6G, $C_{28}H_{31}N_2O_3Cl$, 99%), and crystal violet (CV, $C_{25}H_{30}ClN_3$, 99%) were used directly with no further purification. Deionized water (18 MΩ·cm) was obtained from a Milli-Q water-purification system.

2.2. Synthesis of Ag Nanocubes. Briefly, Ag nanocubes were synthesized according to previous method.[34] In a 20 mL vial, ethylene glycol (5 mL) was first heated in an oil bath and kept at 140 °C for 1 h. Then, 1 mL of HCl (3 M) and 100 μL of $CO(NH_2)_2$ (0.39 M) were added into the above solution under vigorous stirring for 20 min. Then, the ethylene glycol solutions of $AgNO_3$ (99.13 mM, 3 mL) and PVP (155 mM in terms of the repeat unit, 3 mL) were simultaneously injected to the above solution under continuous stirring for 50, 100, and 120 min for the production of Ag nanocubes with different sizes. The as-obtained Ag nanocubes were aged in deionized water at 25 °C for a week for the formation of Ag nanocubes with truncated corners. Nonuniform Ag nanocubes were a mixture of different sizes of sharp edge/corner and truncated ones. All samples were washed with acetone and water three times to remove excess ethylene glycol and PVP for the morphological and structural characterization.

2.3. Preparation of Si Substrate. Si substrate was used for the deposition of Ag nanocubes and probe molecule (Ag/Si substrate). The Si substrate was cleaned by deionized water, sulfuric acid, hydrogen peroxide, and deionized water, in sequence.

2.4. Preparation of Ag/PE/Au Film. Ag/PE/Au film was prepared by a layer-by-layer deposition method. First, Au film (50 nm) with a Cr adhesion layer (5 nm) was sputtered onto a Si substrate via a magnetron sputtering apparatus (MSP-620). Second, the Au film was alternatively immersed into the cationic polyelectrolyte solution of PAH (0.003 mol of monomer/L)/NaCl (1 M) and anionic polyelectrolyte solution of PSS (0.003 mol of monomer/L)/NaCl (1 M) for 30 min. After each immersion, Au film was thoroughly rinsed with deionized water, soaked in deionized water for 1 min, and further immersed in NaCl solution (1 M) for 30 s. It should be noted that the outermost layer was PAH for the assembly of each PE layer. Moveover, Au film was dried with a stream of nitrogen before the next PE layer deposition. Ag nanocubes were immobilized on the PE surface by bringing the PE-coated Au film face-down into contact with Ag nanocubes solution, following by rinsing with deionized water and drying under a stream of high-purity nitrogen. The coverage of Ag nanocubes on Au film can be modulated by adjusting the concentration of Ag nanocubes solution and the deposition time. The as-prepared Au films were fully rinsed with deionized water and dried under a continuous flow of high-purity nitrogen.

2.5. Characterization. The ultraviolet−visible (UV−vis) extinction spectra were acquired at room temperature by a Lambda 750S spectrometer. Transmission electron microscopy (TEM) studies were performed with a Hitachi 7650, and scanning electron microscopy (SEM) images were acquired with a JSM-7500F. Raman spectra were collected with a HR800 Raman spectrometer (Horiba Jobin Yvon). The excitation wavelength was 633 nm with a laser spot size of ∼2 μm and a power of 1.71 mW.

2.6. SERS Measurements. R6G and CV were used as probe molecules. The as-prepared Ag/PE/Au substrate was immersed in the probe molecules solution (10^{-2}−10^{-11} M) for 1 h and then thoroughly rinsed with deionized water to remove the free probe molecules. For silicon substrates, Ag nanocubes was mixed with probe molecules solution to reach a final concentration and left the mixtures there for 5 h. Then, the different concentrations of probe molecules was dropped onto the precleaned Si substrate. Laser wavelength: 633 nm; power: 1.71 mW; lens: 100× objective; acquisition time: 3 s. For each SERS spectrum, we measured 20 SERS spectra on randomly chosen positions of the substrate and then took the average values of them.

2.7. Theoretical Simulations. Finite-difference time-domain (FDTD) simulations were performed with a simulated Ag/PE/Au assembly with a periodic structure of transversal translation. The outermost layer of the Ag/PE/Au sandwiched structure is covered with Ag nanocubes. The geometric parameter of the Ag nanocube is set at 60, 90, and 115 nm. In addition, the thicknesses of Au film (bottom layer) and Si substrate are fixed at 50 and 100 nm along the *z*-direction, respectively. The PE gap (middle layer) between the Ag nanocube and Au film (Ag nanocubes/PE/Au film) is set at 0, 4, 8, and 12 nm. The complex refractive indexes of Ag, Au, and polyelectrolyte are adopted from tabulated values measured by Johnson and Christy. The medium outside of Ag/PE/Au sandwiched structure film was an atmospheric environment. Periodic boundary conditions were applied along the *x*- and *y*-directions while perfectly matched layers (PML) boundary conditions were utilized along the *z*-direction. A plane wave (300−2000 nm, linear polarized light) with the electric field parallel to the *x*-axis illuminated normally the periodic structure along the −z-direction. A conform mesh technique is employed to mesh the structure and the minimum mesh is set at 0.5 × 0.5 × 0.5 nm^3. The localized electric field distribution of the Ag/PE/Au structures on the $y = 0$ plane (excitation wavelength, 633 nm) is collected by the field monitor.

3. RESULTS AND DISCUSSION

Ag nanocubes with different sizes and morphologies are successfully synthesized by a recently developed method, which involved the use of carbamide as the additive/promoter.[34] Figure 1a demonstrates a representative SEM image of truncated Ag nanocubes in comparison with the freshly prepared Ag nanocubes (Figure 1b and Figure S1a,b). XRD measurements confirmed the formation of Ag nanocubes. As presented in Figure 1c, all samples exhibited four major peaks at 2θ = 38.1°, 44.3°, 64.4°, and 77.5°, corresponding to (111), (200), (220), and (311) planes of face-centered cubic (fcc) Ag nanocystals.[32,33] The corresponding size distributions of Ag nanocubes are included in the insets of Figure 1d−f. The SEM and XRD characterization confirmed the formation of Ag nanocubes, indicating that the facets of Ag nanocubes were primarily composed of (200) planes.[40,41] After the formation of truncated Ag nanocubes, the peak intensity of the (200) plane decreased in comparison to the case of sharp Ag nanocubes. It should be noted that the size of Ag nanocubes

https://dx.doi.org/10.1021/acsanm.9b02579
ACS Appl. Nano Mater. 2020, 3, 1934−1941

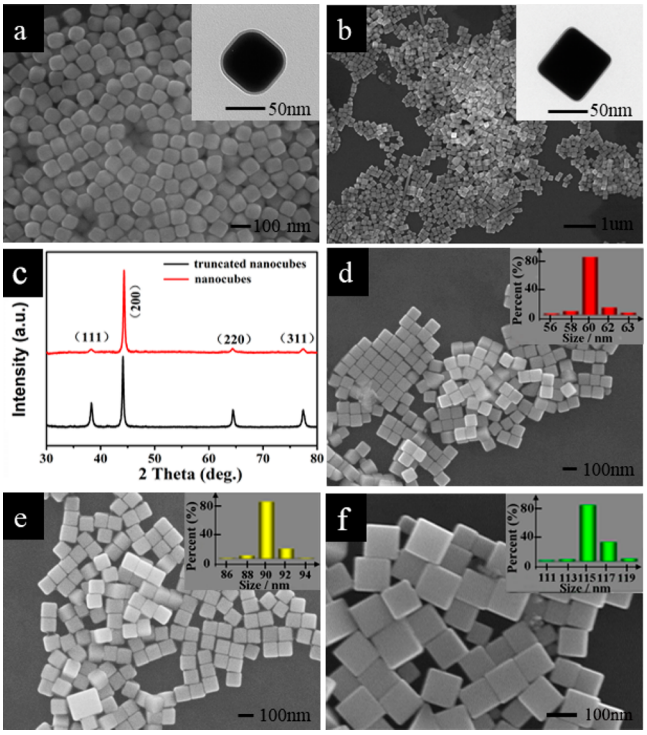

Figure 1. SEM image of (a) truncated Ag nanocubes and (b) freshly prepared Ag nanocubes. Insets are the TEM images of a single Ag nanocube. (c) XRD patterns of freshly prepared Ag nanocubes and truncated Ag nanocubes. SEM images of Ag nanocubes collected at the reaction times of (d) 50, (e) 100, and (f) 120 min.

can be modified by the reaction time. From Figure 1d–f, it can be seen that the edge length of as-synthesized Ag nanocubes could be tuned from 60 to 90 and 115 nm by increasing the reaction time of from 50 to 100 and 120 min, respectively. It should be pointed out that all Ag nanocubes had a uniform edge length with small variations (≤5 nm).

The optical properties of Ag nanocubes were characterized by UV–vis absorption measurements. The UV–vis spectra of Ag nanocubes with different sizes (Figure 1d–f) are shown in Figure 2, demonstrating Ag nanocubes (edge length ~60 nm) exhibited a greenish color while other nanocubes were found to be brown (edge length ~90 nm) and yellow (edge length

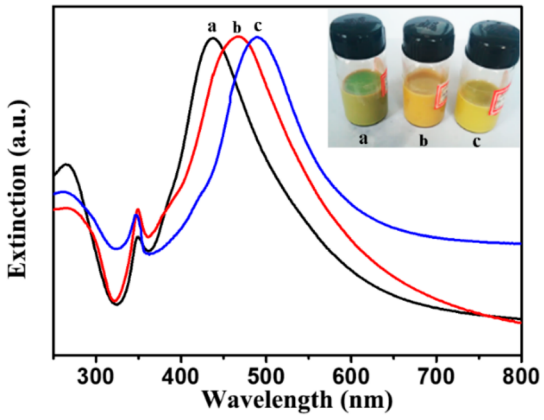

Figure 2. UV–vis absorption spectra of as-prepared Ag nanocubes of different edge lengths: (a) 60, (b) 90, and (c) 115 nm. Inset shows the corresponding photograph.

~115 nm). It should be mentioned that all Ag nanocubes exhibited two prominent absorption peaks. On the one hand, the sharp one at 345 nm can be attributed to the SPR of the corners and edges of uniform Ag nanocubes. On the other hand, the second one is much broader and more intense, which is ascribed to the major LSP resonance of the (100) plane of fcc Ag nanocubes.[42−45] As the size of Ag nanocubes increased from 60 to 90 and 115 nm, the LSP resonance peak displayed an apparent red-shift from 434 to 462 and 479 nm, respectively.

The as-prepared Ag nanocubes were assembled onto a PE surface which deposited on the Au film (see Figure 3). No

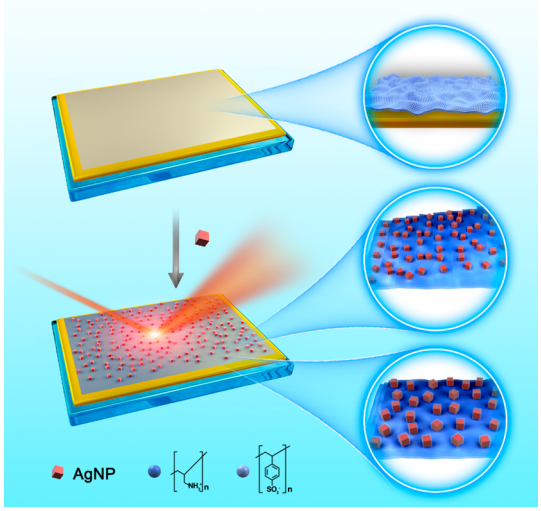

Figure 3. Schematic illustration of Ag/PE/Au sandwich-structured film. First, the Au film was functionalized with dielectric spacer. Second, Ag nanocubes were immobilized by electrostatic attraction.

obvious agglomeration was observed as the Ag nanocubes solution concentration was lower than 10 mM (Figure S2a). However, Ag nanocubes were found be agglomerated on the PE/Au film regardless of the time of deposition as the high concentration of Ag nanocubes solution was used (see Figure S2b). Moreover, the coverage of Ag nanocubes on the Au film was modulated by prolonging the deposition time. It should be noted that partial agglomeration of Ag nanocubes was observed as the deposition time extended to 90 min (Figure S3b). As exhibited in Figure 4a,b, the SEM characterizations revealed that both of the as-prepared and truncated Ag nanocubes can be randomly adsorbed on the PE surface without apparent agglomeration. Although nonuniform Ag nanocubes (Figure S1c) can be adsorbed onto the PE/Au film as well, partial aggregation can be observed (Figure 4c).

The application of the Ag/PE/Au sandwich-structured substrate as a SERS substrate was examined by using R6G and CV as the analyte molecules. It should be mentioned that no distinct Raman signals of R6G were observed without any metal substrate even at the R6G concentration as high as 10^{-2} M (see Figure S4). Yet, by using freshly prepared Ag nanocubes deposited on a Si surface (Ag/Si), we can clearly detect well-defined Raman signals (Table S1). As shown in Figure S5a, the detect limit of R6G was found to be 10^{-9} M. Furthermore, the SERS enhancement was found to vary with the morphology of Ag nanocubes. The freshly prepared Ag nanocubes exhibited the highest Raman enhancement in comparison with truncated and nonuniform Ag nanocubes

https://dx.doi.org/10.1021/acsanm.9b02579
ACS Appl. Nano Mater. 2020, 3, 1934−1941

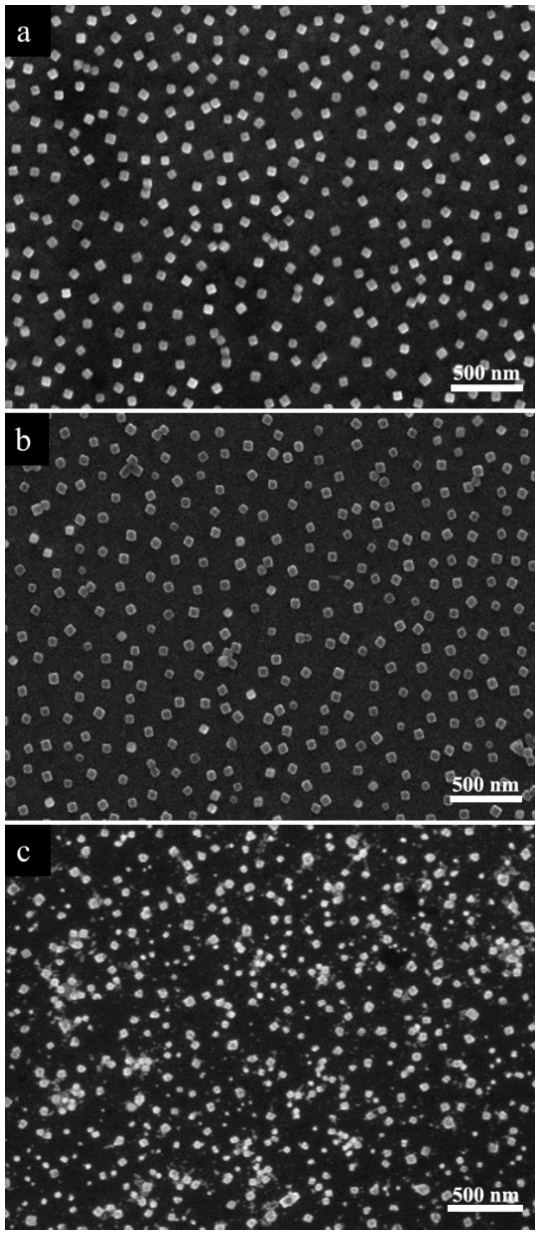

Figure 4. SEM images of Ag nanocubes/PE/Au film: (a) freshly prepared nanocubes, (b) truncated nanocubes, and (c) nonuniform nanocubes, obtained with fixed initial concentration (10 mM) and deposition time (60 min).

(see Figure S5b). As shown in Figure 1c, the XRD analysis indicated the enhanced SERS performance originated from the morphology control rather than the change of crystal structure of Ag nanocubes.

Further enhancement was achieved by using the Ag/PE/Au sandwich-structured substrate. From Figure S6, it can be seen that the SERS sensitivity of Ag/PE/Au substrate was about 2 times higher than that of Ag/Si substrate alone, and the detection limit of R6G by using the Ag/PE/Au substrate was found to be at the 10^{-10} M level (Figure S7). There was no Raman peak of R6G without Ag nanocubes, indicating that Ag nanocubes played a vital role in SERS activity. Furthermore, we found that Ag/PE/Au substrate also demonstrated excellent Raman enhancement for CV with a detection limit up to 10^{-10} M as well (Figure S8 and Table S2). The Raman signal enhancement became intensified by decreasing the size of the freshly prepared Ag nanocubes from 115 to 60 nm, as shown in Figure 5a. This can be ascribed to the fact that smaller Ag nanocubes contain a larger fraction of sharp edges and corners, acting as the "hot spots" for SERS.[13,41,46] The number of probe molecules adsorbed on surface of Ag nanocubes also increased with decreasing size. Figure 5b (R6G) and Figures S9 and S10 (CV) demonstrated the SERS spectra with different numbers of PE layers in the Ag/PE/Au sandwiched-structured substrate. We found that the sensitivity of the Raman signals first increases and then decreases with the increase thickness of the PE layer while reaching a maximum signal at three layers of PE. The same feature also appears in the Ag/PE/Au substrate built by truncated Ag nanocubes for both R6G and CV molecular (Figure S10). In fact, for the nonuniform nanocubes deposited on PE/Au film, there was no regulation to follow due to the uncontrollable agglomeration of nanoparticles on the PE surface (see Figure S11). For the sandwich-structured film, the collective oscillation of electrons gathered in the waveguide cavity between Ag nanocubes and Au film.[30] The electromagnetic field was centrally localized within the gap between Ag nanocubes and Au film due to the hybridization of LSP and SPP resonance. Moreover, the PE spacer between Au film and Ag nanocubes acted as phase retarder, leading to a stronger SERS singal.[47]

In fact, the observed resonances could be viewed as waveguide modes in the sandwiched structure where electromagnetic energy can reflect back and forth with the assistant of the underlying Au film as a mirror.[48−50] The above-mentioned results indicated that the coupling strength between the LSP and SPP resonance could be precisely tuned by regulating the thickness of PE layer and the morphology or size of Ag nanocubes.[40] The generation of high *E*-field enhancements through the design of plasmonic nanostructure facilitated the rapid and sensitive SERS detection of target analytes.[10]

Although the high enhancement factors have been reported for various nanostructured substrates, it remains a challenge to achieve a high reproducibility of SERS measurements. To evaluate the repeatability for as-fabricated SERS substrate, we randomly selected four different points on the Ag/PE/Au substrate (Figure S12). There were no obvious changes in the intensity of characteristic Raman peaks of R6G at 610 and 1650 cm^{-1}, indicating the assembly of Ag/PE/Au substrate provided a potential strategy for application in the near future.

To verify our experimental results, FDTD simulations were performed to examine the influence the electric field intensity in the PE spacer at different thicknesses. Figure 6 demonstrates a dynamic process of the cross section of the spatial electric field distribution at the excitation wavelength of 633 nm while increasing the distance between Ag nanocube (60 nm) and Au film. The *E*-field distribution without the involvement of PE layer was found to be located at the upper corners of the Ag nanocube (Figure 6a). As the distance between the Ag nanocube and Au film increased to 4 nm, which refers to three layers of PE, there was a strong *E*-field located at the cavity defined by the Ag nanocube and Au film (Figure 7b). The SERS enhancement factor is proportional to $|E/E_0|$ due to the increased hot spots for SERS.[4] As the gap is further increased (8 to 12 nm, ≥4 layers; see Figure 6c,d), the *E*-field intensity was actually subdued, indicating an optimal gap layer thickness for the Ag/PE/Au substrate. As demonstrated in Figure 6, the greatest enhancement was observed with three PE layers in the Ag/PE/Au sandwich-structured substrate.

https://dx.doi.org/10.1021/acsanm.9b02579
ACS Appl. Nano Mater. 2020, 3, 1934−1941

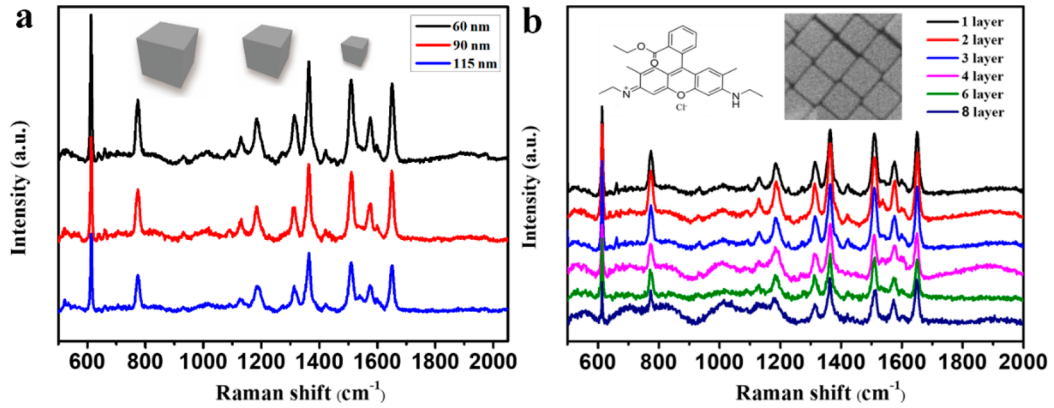

Figure 5. SERS spectra of R6G solution (10^{-7} M) based on Ag/PE/Au sandwich-structured substrate (three layers) (a) with freshly prepared Ag nanocubes of different sizes and (b) with different numbers of PE layers.

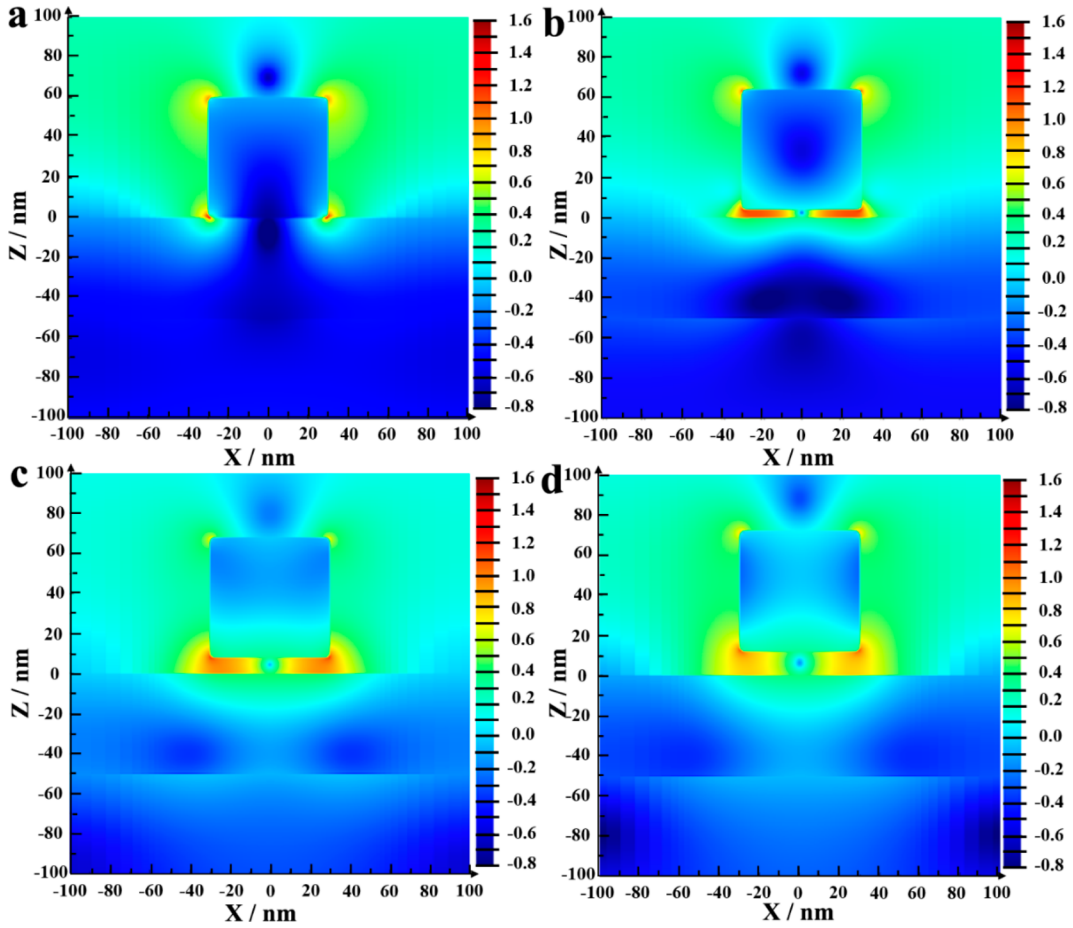

Figure 6. Simulation models of the Ag/PE/Au substrate with different gaps are built. The corresponding *E*-field distribution of Ag/PE/Au substrate calculated with the FDTD method is shown in a (0 nm), b (4 nm), c (8 nm), and d (12 nm); the scale bar at the right for the magnetic field enhancement. The polarization of the incident laser is along this plane.

The corresponding *E*-field distribution of Ag/PE/Au substrate is shown in Figure 7. The polarization of the incident laser was along the *XZ*-plane. Numerical simulations were also performed to further verify the size influence of Ag nanocube to the electric field intensity. As shown in Figure 7, the electric field intensity decreased gradually with increasing the size of nanocube. The 60 nm Ag nanocubes exhibited a much stronger *E*-field intensity than the larger ones (e.g., 90 and 115 nm). The simulation results agreed well with our experimental results, which are presented in Figure S13.

4. CONCLUSIONS

In summary, Ag nanoparticles were synthesized in large quantities with different size and morphology. The Ag nanocubes/polyelectrolyte/Au sandwich-structured film was facilely fabricated and then employed as SERS substrate with reproducible and uniform SERS activity. The electromagnetic enhancement resulted from the strong coupling of multiple LSP and SPP resonances between adjacent Ag nanocubes and between Ag nanocubes and Au film. The FDTD simulations

https://dx.doi.org/10.1021/acsanm.9b02579
ACS Appl. Nano Mater. 2020, 3, 1934−1941

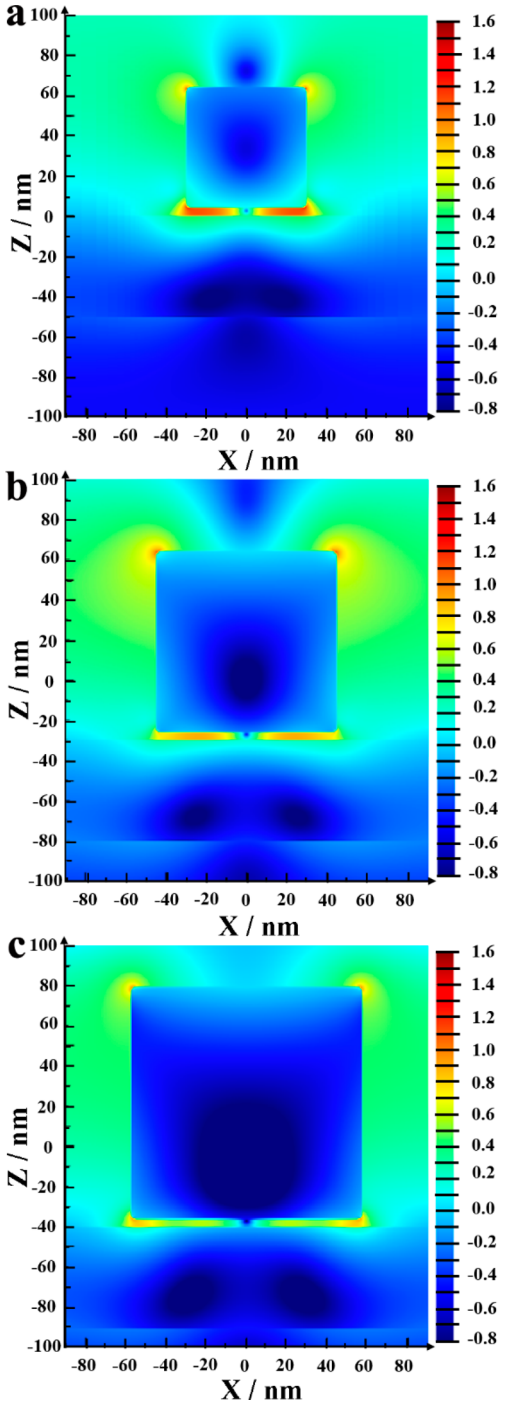

Figure 7. Simulation models of the Ag/PE/Au substrate with different Ag nanocube sizes (gap = 4 nm): a (60 nm), b (90 nm), and c (115 nm); scale bar at the right for the magnetic field strength.

further revealed the enhancement of the electrical field strength within the polyelectrolyte gap layer, where the optimized gap thickness was identified to be three polyelectrolyte layers. In this work, we demonstrate that Ag nanocubes/polyelectrolyte/Au sandwich-structured film can be considered as an inexpensive and sensitive SERS substrate in practical sensing applications.

■ ASSOCIATED CONTENT

Supporting Information

The Supporting Information is available free of charge at https://pubs.acs.org/doi/10.1021/acsanm.9b02579.

SEM and TEM images, Raman spectra, and results of theoretical simulations as noted in the text (PDF)

■ AUTHOR INFORMATION

Corresponding Authors

Yang Zhang − *Beijing Institute of Nanoenergy and Nanosystems, Chinese Academy of Sciences, Beijing 100083, China;* orcid.org/0000-0002-3002-4367; Email: zhangyang@binn.cas.cn

Jiatao Zhang − *Beijing Key Laboratory of Construction Tailorable Advanced Functional Materials and Green Applications, School of Materials Science and Engineering, Beijing Institute of Technology, Beijing 100081, China;* orcid.org/0000-0001-7414-4902; Email: zhangjt@bit.edu.cn

Changzheng Wang − *Beijing Key Laboratory of Functional Materials for Building Structure and Environment Remediation, Beijing University of Civil Engineering and Architecture, Beijing 100044, China;* orcid.org/0000-0001-9111-6866; Email: changzhwang@163.com

Authors

Qiang Wang − *Laboratory for Micro-sized Functional Materials, College of Elementary Education and Department of Chemistry, Capital Normal University, Beijing 100048, China*

Xiuhui Bai − *Laboratory for Micro-sized Functional Materials, College of Elementary Education and Department of Chemistry, Capital Normal University, Beijing 100048, China*

Ziang Zhou − *Laboratory for Micro-sized Functional Materials, College of Elementary Education and Department of Chemistry, Capital Normal University, Beijing 100048, China*

Ming Guo − *Laboratory for Micro-sized Functional Materials, College of Elementary Education and Department of Chemistry, Capital Normal University, Beijing 100048, China*

Chunhong Li − *National Laboratory for Superconductivity, Institute of Physics and Beijing National Laboratory for Condensed Matter Physics, Chinese Academy of Sciences, Beijing 100190, China*

Shaowei Chen − *Department of Chemistry and Biochemistry, University of California, Santa Cruz, Santa Cruz, California 95064, United States;* orcid.org/0000-0002-3668-8551

Complete contact information is available at: https://pubs.acs.org/10.1021/acsanm.9b02579

Author Contributions

Q.W. and X.B. contributed equally to this work.

Notes

The authors declare no competing financial interest.

■ ACKNOWLEDGMENTS

This work was supported by the National Natural Science Foundation of China (NSFC Nos. 21471103 and 21603014), the Beijing Municipal Commission of Education (No. 19530050182), and the State Key Laboratory of Explosion Science and Technology (ZDKT18-01, Beijing Institute of Technology).

REFERENCES

(1) You, L.; Li, R.; Dong, X.; Wang, F.; Guo, J.; Wang, C. Micron-Sized Surface Enhanced Raman Scattering Reporter/Fluorescence Probe Encoded Colloidal Microspheres for Sensitive DNA Detection. *J. Colloid Interface Sci.* **2017**, *488*, 109−117.

(2) Li, J. L.; Sun, D. W.; Pu, H.; Jayas, D. S. Determination of Trace Thiophanate-Methyl and Its Metabolite Carbendazim with Teratogenic Risk in Red Bell Pepper (Capsicumannuum L.) by Surface-Enhanced Raman Imaging Technique. *Food Chem.* **2017**, *218*, 543−552.

(3) Miljanic, S.; Ratkaj, M.; Matkovic, M.; Piantanida, I.; Gratteri, P.; Bazzicalupi, C. Assessment of Human Telomeric G-Quadruplex Structures Using Surface-Enhanced Raman Spectroscopy. *Anal. Bioanal. Chem.* **2017**, *409*, 2285−2295.

(4) Fleischmann, M.; Hendra, P. J.; McQuillan, A. J. Raman Spectra of Pyridine Adsorbed at a Silver Electrode. *Chem. Phys. Lett.* **1974**, *26*, 163−166.

(5) Yang, S.; Dai, X.; Stogin, B. B.; Wong, T. S. Ultrasensitive Surface-Enhanced Raman Scattering Detection in Common Fluids. *Proc. Natl. Acad. Sci. U. S. A.* **2016**, *113*, 268−73.

(6) Kneipp, J.; Kneipp, H.; Kneipp, K. SERS-A Single-Molecule and Nanoscale Tool For Bioanalytics. *Chem. Soc. Rev.* **2008**, *37*, 1052−1060.

(7) Masim, F. C. P.; Porta, M.; Hsu, W.-H.; Nguyen, M. T.; Yonezawa, T.; Balčytis, A.; Juodkazis, S.; Hatanaka, K. Au Nanoplasma as Efficient Hard X-ray Emission Source. *ACS Photonics* **2016**, *3*, 2184−2190.

(8) Shanmukh, S.; Jones, L.; Driskell, J.; Zhao, Y.; Dluhy, R.; Tripp, R. A. Rapid and Sensitive Detection of Respiratory Virus Molecular Signatures Using a Silver Nanorod Array SERS Substrate. *Nano Lett.* **2006**, *6*, 2630−2636.

(9) Yin, Z.; Wang, Y.; Song, C.; Zheng, L.; Ma, N.; Liu, X.; Li, S.; Lin, L.; Li, M.; Xu, Y.; Li, W.; Hu, G.; Fang, Z.; Ma, D. Hybrid Au-Ag Nanostructures for Enhanced Plasmon-Driven Catalytic Selective Hydrogenation through Visible Light Irradiation and Surface-Enhanced Raman Scattering. *J. Am. Chem. Soc.* **2018**, *140*, 864−867.

(10) Zu, S.; Li, B. W.; Gong, Y. J.; Li, Z. W.; Ajayan, P. M.; Fang, Z. Y. Active Control of Plasmon-Exciton Coupling in MoS_2-Ag Hybrid Nanostructures. *Adv. Opt. Mater.* **2016**, *4*, 1463−1469.

(11) Zhang, Y.; Shoaib, A.; Li, J. J.; Ji, M. W.; Liu, J. J.; Xu, M.; Tong, B.; Zhang, J. T.; Wei, Q. Plasmon Enhanced Photoelectrochemical Sensing of Mercury (II) ions in Human Serum Based on Au@Ag Nanorods Modified TiO_2 Nanosheets Film. *Biosens. Bioelectron.* **2016**, *79*, 866−873.

(12) Campion, A.; Kambhampati, P. Surface-Enhanced Raman Scattering. *Chem. Soc. Rev.* **1998**, *27*, 241−250.

(13) De Angelis, F.; Patrini, M.; Das, G.; Maksymov, I.; Galli, M.; Businaro, L.; Andreani, L. C.; Di Fabrizio, E. A Hybrid Plasmonic-Photonic Nanodevice for Label-Free Detection of a Few Molecules. *Nano Lett.* **2008**, *8*, 2321−2327.

(14) Nie, S. M.; Emery, S. R. Probing Single Molecules and Single Nanoparticles by Surface-Enhanced Raman Scattering. *Science* **1997**, *275*, 1102−1106.

(15) Chen, H. J.; Sun, Z. H.; Ni, W. H.; Woo, K. C.; Lin, H. Q.; Sun, L. D.; Yan, C. H.; Wang, J. F. Plasmon Coupling in Clusters Composed of Two-Dimensionally Ordered Gold Nanocubes. *Small* **2009**, *5*, 2111−2119.

(16) Woo, K. C.; Shao, L.; Chen, H. J.; Liang, Y.; Wang, J. F.; Lin, H. Q. Universal Scaling and Fano Resonance in the Plasmon Coupling between Gold Nanorods. *ACS Nano* **2011**, *5*, 5976−5986.

(17) Ming, T.; Chen, H. J.; Jiang, R. B.; Li, Q.; Wang, J. F. Plasmon-Controlled Fluorescence: Beyond the Intensity Enhancement. *J. Phys. Chem. Lett.* **2012**, *3*, 191−202.

(18) Fang, Z. Y.; Zhu, X. Plasmonics in Nanostructures. *Adv. Mater.* **2013**, *25*, 3840−3856.

(19) Rycenga, M.; Xia, X.; Moran, C. H.; Zhou, F.; Qin, D.; Li, Z.-Y.; Xia, Y. Generation of Hot Spots with Silver Nanocubes for Single-Molecule Detection by Surface-Enhanced Raman Scattering. *Angew. Chem., Int. Ed.* **2011**, *50*, 5473−5477.

(20) McLellan, J. M.; Li, Z. Y.; Siekkinen, A. R.; Xia, Y. N. The SERS Activity of a Supported Ag Nanocube Strongly Depends on Its Orientation Relative to Laser Polarization. *Nano Lett.* **2007**, *7*, 1013−1017.

(21) Liebig, F.; Sarhan, R. M.; Sander, M.; Koopman, W.; Schuetz, R.; Bargheer, M.; Koetz, J. Deposition of Gold Nanotriangles in Large Scale Close-Packed Monolayers for X-ray-Based Temperature Calibration and SERS Monitoring of Plasmon-Driven Catalytic Reactions. *ACS Appl. Mater. Interfaces* **2017**, *9*, 20247−20253.

(22) Cao, Y.; Guo, J.; Shi, R.; Waterhouse, G. I. N.; Pan, J.; Du, Z.; Yao, Q.; Wu, L.-Z.; Tung, C.-H.; Xie, J.; Zhang, T. Evolution of Thiolate-Stabilized Ag Nanoclusters from Ag-Thiolate Cluster Intermediates. *Nat. Commun.* **2018**, *9*, 2379.

(23) Yang, Y.; Lee, Y. H.; Phang, I. Y.; Jiang, R.; Sim, H. Y. F.; Wang, J.; Ling, X. Y. A Chemical Approach To Break the Planar Configuration of Ag Nanocubes into Tunable Two-Dimensional Metasurfaces. *Nano Lett.* **2016**, *16*, 3872−3878.

(24) Khlebtsov, B. N.; Khanadeev, V. A.; Panfilova, E. V.; Bratashov, D. N.; Khlebtsov, N. G. Gold Nanoisland Films as Reproducible SERS Substrates for Highly Sensitive Detection of Fungicides. *ACS Appl. Mater. Interfaces* **2015**, *7*, 6518−6529.

(25) Gunnarsson, L.; Bjerneld, E. J.; Xu, H.; Petronis, S.; Kasemo, B.; Kall, M. Interparticle Coupling Effects in Nanofabricated Substrates for Surface-Enhanced Raman Scattering. *Appl. Phys. Lett.* **2001**, *78*, 802−804.

(26) Kalachyova, Y.; Mares, D.; Jerabek, V.; Zaruba, K.; Ulbrich, P.; Lapcak, L.; Svorcik, V.; Lyutakov, O. The Effect of Silver Grating and Nanoparticles Grafting for LSP-SPP Coupling and SERS Response Intensification. *J. Phys. Chem. C* **2016**, *120*, 10569−10577.

(27) Farhang, A.; Bigler, N.; Martin, O. J. Coupling of Multiple LSP And SPP Resonances: Interactions Between an Elongated Nanoparticle and a Thin Metallic Film. *Opt. Lett.* **2013**, *38*, 4758−4761.

(28) Mock, J. J.; Hill, R. T.; Degiron, A.; Zauscher, S.; Chilkoti, A.; Smith, D. R. Distance-Dependent Plasmon Resonant Coupling between a Gold Nanoparticle and Gold Film. *Nano Lett.* **2008**, *8*, 2245−2252.

(29) Nishijima, Y.; Hashimoto, Y.; Rosa, L.; Khurgin, J. B.; Juodkazis, S. Scaling Rules of SERS Intensity. *Adv. Opt. Mater.* **2014**, *2*, 382−388.

(30) Moreau, A.; Ciraci, C.; Mock, J. J.; Hill, R. T.; Wang, Q.; Wiley, B. J.; Chilkoti, A.; Smith, D. R. Controlled-Reflectance Surfaces with Film-Coupled Colloidal Nanoantennas. *Nature* **2012**, *492*, 86−89.

(31) Zhou, S.; Li, J.; Gilroy, K. D.; Tao, J.; Zhu, C.; Yang, X.; Sun, X.; Xia, Y. Facile Synthesis of Silver Nanocubes with Sharp Corners and Edges in an Aqueous Solution. *ACS Nano* **2016**, *10*, 9861−9870.

(32) Xia, Y.; Gilroy, K. D.; Peng, H. C.; Xia, X. Seed-Mediated Growth of Colloidal Metal Nanocrystals. *Angew. Chem., Int. Ed.* **2017**, *56*, 60−95.

(33) Sanchez-Iglesias, A.; Winckelmans, N.; Altantzis, T.; Bals, S.; Grzelczak, M.; Liz-Marzan, L. M. High-Yield Seeded Growth of Monodisperse Pentatwinned Gold Nanoparticles through Thermally Induced Seed Twinning. *J. Am. Chem. Soc.* **2017**, *139*, 107−110.

(34) Zhang, J.; Wang, Q.; Zhang, X.; Wang, J.; Guo, M.; Wiley, B. J.; Li, C.; Hu, C. Carbamide Promoted Polyol Synthesis and Transmittance Properties of Silver Nanocubes. *Inorg. Chem. Front.* **2016**, *3*, 547−555.

(35) Bai, X.; Wang, J.; Guo, M.; Li, Z.; Chen, N.; Wang, Q.; Li, C.; Wang, C.; Dong, K.; Chen, S. Surfaces Enhanced with Film-Coupled Silver Nanopolyhedrons for Optical Transmittance. *RSC Adv.* **2017**, *7*, 39299−39305.

(36) Ciraci, C.; Hill, R. T.; Mock, J. J.; Urzhumov, Y.; Fernandez-Dominguez, A. I.; Maier, S. A.; Pendry, J. B.; Chilkoti, A.; Smith, D. R. Probing the Ultimate Limits of Plasmonic Enhancement. *Science* **2012**, *337*, 1072−1074.

(37) Lassiter, J. B.; McGuire, F.; Mock, J. J.; Ciraci, C.; Hill, R. T.; Wiley, B. J.; Chilkoti, A.; Smith, D. R. Plasmonic Waveguide Modes of Film-Coupled Metallic Nanocubes. *Nano Lett.* **2013**, *13*, 5866−5872.

https://dx.doi.org/10.1021/acsanm.9b02579
ACS Appl. Nano Mater. 2020, 3, 1934−1941

(38) Chen, W.; Zhang, S.; Deng, Q.; Xu, H. Probing of Sub-Picometer Vertical Differential Resolutions Using Cavity Plasmons. *Nat. Commun.* **2018**, *9*, 801.
(39) Johnson, P. B.; Christy, R. W. Optical Constants of the Noble Metals. *Phys. Rev. B* **1972**, *6*, 4370−4379.
(40) Li, D.; Shan, Y.; Liu, R.; Wu, Q.; Zheng, T.; Li, K. Facile Preparation of Ag Nanocubes At 30°C Under Light Irradiation. *Micro Nano Lett.* **2018**, *13*, 494−497.
(41) Siekkinen, A. R.; McLellan, J. M.; Chen, J.; Xia, Y. Rapid Synthesis of Small Silver Nanocubes by Mediating Polyol Reduction with a Trace Amount of Sodium Sulfide or Sodium Hydrosulfide. *Chem. Phys. Lett.* **2006**, *432*, 491−496.
(42) Zhang, Q.; Li, W.; Moran, C.; Zeng, J.; Chen, J.; Wen, L.-P.; Xia, Y. Seed-Mediated Synthesis of Ag Nanocubes with Controllable Edge Lengths in the Range of 30−200 nm and Comparison of Their Optical Properties. *J. Am. Chem. Soc.* **2010**, *132*, 11372−11378.
(43) Duan, G.; Cai, W.; Luo, Y.; Li, Z.; Li, Y. Electrochemically Induced Flowerlike Gold Nanoarchitectures and Their Strong Surface-Enhanced Raman Scattering Effect. *Appl. Phys. Lett.* **2006**, *89*, 211905.
(44) Zhang, Q.; Li, W.; Wen, L. P.; Chen, J.; Xia, Y. Facile Synthesis of Ag Nanocubes of 30 to 70 nm in Edge Length with CF_3COOAg as a Precursor. *Chem. - Eur. J.* **2010**, *16*, 10234−10239.
(45) Michaels, A. M.; Nirmal, M.; Brus, L. E. Surface Enhanced Raman Spectroscopy of Individual Rhodamine 6G Molecules on Large Ag Nanocrystals. *J. Am. Chem. Soc.* **1999**, *121*, 9932−9939.
(46) Benz, F.; Chikkaraddy, R.; Salmon, A.; Ohadi, H.; de Nijs, B.; Mertens, J.; Carnegie, C.; Bowman, R. W.; Baumberg, J. J. SERS of Individual Nanoparticles on a Mirror: Size Does Matter, but so Does Shape. *J. Phys. Chem. Lett.* **2016**, *7*, 2264−2269.
(47) Zheng, Y.; Rosa, L.; Thai, T.; Ng, S. H.; Juodkazis, S.; Bach, U. Phase Controlled SERS Enhancement. *Sci. Rep.* **2019**, *9*, 744.
(48) Barnett, S. M.; Harris, N.; Baumberg, J. J. Molecules In The Mirror: How SERS Backgrounds Arise from the Quantum Method of Images. *Phys. Chem. Chem. Phys.* **2014**, *16*, 6544−6549.
(49) Daniels, J. K.; Chumanov, G. Nanoparticle-Mirror Sandwich Substrates for Surface-Enhanced Raman Scattering. *J. Phys. Chem. B* **2005**, *109*, 17936−17942.
(50) Mubeen, S.; Zhang, S.; Kim, N.; Lee, S.; Krämer, S.; Xu, H.; Moskovits, M. Plasmonic Properties of Gold Nanoparticles Separated from a Gold Mirror by an Ultrathin Oxide. *Nano Lett.* **2012**, *12*, 2088−2094.

https://dx.doi.org/10.1021/acsanm.9b02579
ACS Appl. Nano Mater. 2020, 3, 1934−1941